Biofunctionalized Phospholipid-Capped Mesoporous Silica Nanoshuttles for Targeted Drug Delivery: Improved Water Suspensibility and Decreased Nonspecific Protein Binding

Li-Sheng Wang,[†] Li-Chen Wu,[‡,⊥,*] Shin-Yi Lu,[†] Li-Ling Chang,[§] I-Ting Teng,[†] Chia-Min Yang,[§,⊥,*] and Ja-an Annie Ho[†,⊥,*]

[†]BioAnalytical Lab, Department of Chemistry, National Tsing Hua University, Hsinchu 30013, Taiwan, [‡]Department of Applied Chemistry, National Chi Nan University, Puli, Nantou 54561, Taiwan, and [§]Department of Chemistry, National Tsing Hua University, Hsinchu 30013, Taiwan. [⊥]These authors contributed equally to this work.

ABSTRACT A main challenge in nanobiomedicine is the engineering of nanostructures or nanomaterials that can efficiently encapsulate drugs at high load, cross cell membranes, and controllably release their cargo at target sites. Although mesoporous silica nanoparticles (MSNs) are safe, versatile, and promising carrier materials for targeted drug delivery, their aggregation phenomena under physiological conditions (or salt-containing environments) and their nonspecific binding in protein-containing solutions (or serum) limit their applications in biological science and biomedicine. To address this challenge, we have developed a novel delivery system, termed a nanoshuttle, comprising a nanoscale PEGylated-phospholipid coating and 13-(chlorodimethylsilylmethyl)heptacosane-derivatized MSNs, in which therapeutic or imaging agents may be trapped and ligand-assisted targeted delivery may be achieved through surface functionalization of the phospholipids. As a proof of concept in this study, we selected fluorescein isothiocyanate and folate as the imaging tracer and targeted ligand, respectively. Relative to the bare MSNs, the lipid-capped MSNs exhibited superior suspensibility in phosphate-buffered saline and much lower nonspecific binding *in vitro*. Furthermore, enhanced specific cellular uptake by Hela cells occurred after administering the folate-sensitized phospholipid-capped MSNs. Our results suggest that these highly versatile multifunctional MSNs are promising vectors for nanomedicine applications.

KEYWORDS: mesoporous silica nanoshuttle · water suspensibility · surface functionalization · phospholipids capping · cellular targeting

The application of mesoporous silica nanoparticles (MSNs) as carriers for targeted delivery is a recent development in nanobiotechnology. The unique properties of MSNs—ordered mesopores with tunable pore diameters and structures, large surface areas and pore volumes, high chemical and thermal stabilities, and versatile chemistry for surface functionalization—make them supreme hosts for accommodating guest molecules of various sizes, shapes, and functionalities.[1−6] The past decade has witnessed rapid growth in the application of MSNs in adsorption,[7] catalysis,[8] chemical separations,[9] imaging,[10] targeting,[11] drug delivery,[12] and biosensing.[13] Hosting and stimuli-responsive control release of drugs in MSNs were established by the Lin group, where such systems as quantum dots,[14] gold nanoparticles,[15] iron oxide nanoparticles,[16] and dendrimer[17] were utilized as gates to cap the pores of the MSNs and prevent guest drugs from leaking. Mou and co-workers demonstrated that MSNs labeled with a fluorescent dye could be used as cell markers.[10] Moreover, MSNs modified with gadolinium complexes[18,19] and iron oxides[20,21] have been used in magnetic resonance imaging (MRI). Furthermore, MSNs have also been used to deliver genes,[22] hydrophobic anticancer drugs,[12] and cytochrome *c* into cultured cells.[23]

Although MSNs are potentially useful in nanomedicine, the dispersibility and inherently low biocompatibility[24] of silica-based nanoparticles limit their bioapplications. Silica has an isoelectric point of *ca.* 2.0; dispersions of silica particles are generally charge-stabilized and may be destabilized to form aggregates in the salt-containing solutions, such as phosphate-buffered saline (PBS) or serum.[12,25] Therefore, rapid silica particle aggregation is often observed—especially when administered intravenously, a frequently used route for targeted drug delivery. Accordingly, these silica-based nanoparticles suffer from poor pharmacokinetics, short blood circulation half-lives, and accumulation in lung capillary vessels.[26,27] Strategies based on surface functionalization—with various functional groups (*e.g.*, amino,[28] carboxyl,[29] thiol,[5] and

*Address correspondence to jaho@mx.nthu.edu.tw, cmyang@mx.nthu.edu.tw, lw25@ncnu.edu.tw.

Received for review October 7, 2009 and accepted July 02, 2010.

Published online July 12, 2010. 10.1021/nn901376h

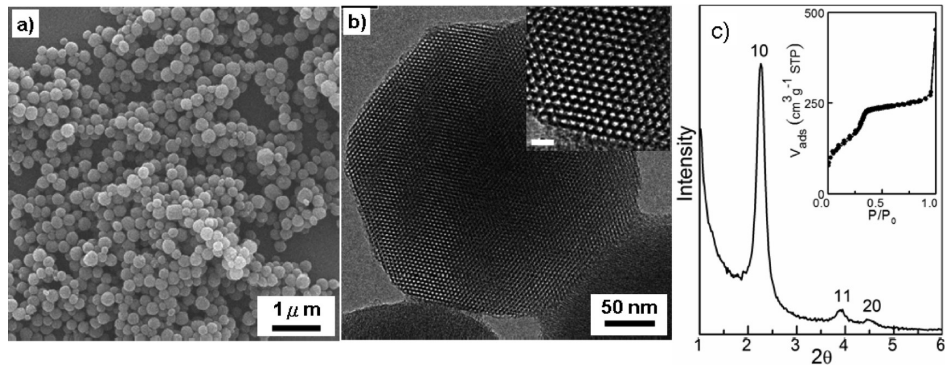

Figure 1. SEM image, (b) TEM image, and (c) PXRD pattern of FMSNs. The length of the scale bar in the inset to panel b is 10 nm. (c inset): N_2 physisorption isotherm of the FMSNs.

phosphonate[30] groups) and large molecules [*e.g.*, block copolymers,[31] poly(ethylene glycol) (PEG),[32] phospholipids[33,34]—have been developed to improve the dispersibility and biocompatibility of silica nanoparticles. Nevertheless, grafted functional groups may be subject to opsonization and remain poorly stable against aggregation;[12,35] large molecules may be present as only low-density surface coatings. Phospholipids, on the other hand, have been used widely to provide biocompatibility and biofunctionality to inorganic nanoparticles.[36−41] PEGylated lipid capping has several advantageous features when used *in vivo*, including increased circulating life, resistance to proteolysis, decreased immunogenicity and/or antigenicity, and excellent repellence of biomolecules. Moreover, because folate receptors are normally expressed at the luminal surfaces of polarized epithelia, which are inaccessible to the circulation,[42,43] but are also found on the surfaces of several cancer cells (*e.g.*, ovarian, endometrial, colorectal, breast, lung, renal cell carcinoma, brain metastases derived from epithelial cancer, and neuroendocrine carcinoma[44]), in this study we employed the folic acid-sensitized phospholipid capping previously developed in our group for the selective delivery of fluorescent MSNs (FMSNs) to distinguish between normal and cancerous cells.[45]

Reports on the preparation and bioapplications of phospholipid-capped MSNs are rare. Very recently, Brinker's group described MSN-supported lipid bilayers for cargo loading, sealing, delivery, and release.[34] For the construction of synergistic "protocell" systems, however, positively charged phospholipids were required for simultaneously fusing with the negatively charged silica surfaces of the MSNs and accommodating the negatively charged dye.[34] Certain types of positively charged phospholipid-based vesicles are, however, toxic, either in cell culture systems[46,47] or *in vivo*,[48,49] restricting their biomedical applications. Because it would be difficult to use other varieties of phospholipids (*i.e.*, other than positively charged ones) to form stable "protocells," in this paper we present a strategy for developing multifunctional nanoshuttles that combine into one system the potential therapeutic and targeting actions with imaging capability. To prove the concept, we synthesized FMSNs exhibiting larger drug loading capacity. Surface attachment with a phospholipid-based capping approach was applied to render the hydrophobic silane-modified FMSNs bioapplicable and to increase the stability of the nanoparticle dispersions in aqueous solution. After characterizing the different formats of the mesoporous silicate, the systems were sensitized with targeting ligands (folic acid) and then tested for their actual *in vitro* applicability. We found that these nanoparticles could be monitored inside living cells using fluorescence imaging and flow cytometric methods, suggesting that they hold great potential as targeting drug delivery vectors. The targeting ligand modification increased the drug payload delivery into human cancer cells relative to that into noncancerous cells. The ability to simultaneously monitor and deliver molecules to targeted tissue regions is likely to be highly beneficial for both imaging and therapeutic purposes.

RESULTS AND DISCUSSION

Synthesis of FMSNs. The synthesized FMSNs had uniform morphology and highly ordered mesostructures. The scanning electron microscopy (SEM) image in Figure 1a reveals that the FMSNs were spherical in shape, having an average diameter of *ca*. 200 nm. In addition, hexagonally packed one-dimensional mesochannels in FMSNs are clearly evident in the transmission electron microscopy (TEM) images in Figure 1b and its inset. In accordance with the TEM observations, the FMSNs gave a well-resolved powder X-ray diffraction (PXRD) pattern (Figure 1c) corresponding to a highly ordered *p6mm* mesostructure. The uniformity of the diameters of the channel-type mesopores was confirmed by the N_2 physisorption measurement (inset to Figure 1c); the sharp step at a relative pressure of 0.30−0.35 corresponds to the phenomena of capillary condensation and evaporation in channel-type mesopores having an

average diameter of 3.7 nm, as evaluated using nonlocal density functional theory (NLDFT).[50] We attribute the step at a relative pressure greater than 0.90 to the textural porosity of the FMSNs. We estimated the surface area and mesopore volume to be 700 $m^2\ g^{-1}$ and 0.44 $cm^3\ g^{-1}$, respectively.

Hydrophobic Modification of FMSNs (m-FMSNs) and PEG-LipoFMSNs. FMSN was reacted with 13-(chlorodimethylsilylmethyl)heptacosane (CDSMH) to render long and hydrophobic carbon chains on the external silica surface. Figure 2 presents Fourier transform infrared (FTIR) spectra of the samples recorded before (FMSN) and after (m-FMSN) functionalization. We observe a C−H stretching absorbance at 2800−3000 cm^{-1} only for the m-FMSNs, suggesting their successful grafting of the hydrophobic heptacocyldimethylsilyl (HDMS) groups. In accordance with their expected surface properties, the m-FMSNs could be dispersed well in $CHCl_3$, but not in aqueous solutions, whereas the FMSNs could be suspended in aqueous solution (see the inset to Figure 2). We used ^{29}Si solid state nuclear magnetic resonance (NMR) spectroscopy to analyze the amounts of the various silicon species present in these samples (Figure 3). For the FMSNs, we observed signals that could be assigned to the various Q^n groups [$Si(OSi)_n(OH)_{4-n}$; $n = 2, 3, 4$] and the FITC-conjugated groups [T groups, $Si(OSi)_n(OH)_{3-n}C$]. The weak relative intensity of the signals for the T groups was due to the low loading of the FITC-conjugated silanes during the co-condensation synthesis of the FMSNs. After functionalization with CDSMH, a new signal attributable to the HDMS groups [M groups, $Si(OSi)C_3$] appeared at *ca.* 14 ppm, accompanied by a decrease in the relative intensities of the Q^2 and Q^3 signals and an increase of that of Q^4 signal. For the m-FMSNs, the *M*/*Q* ratio derived from its spectrum was *ca.* 2.5%, suggesting a small amount of HDMS groups in this sample. Relative to other silanes,[51−54] this very low degree of surface grafting with HDMS groups might be attributable to the difficulty that the relatively bulky HDMS groups have in diffusing into the channel-type mesopores. Indeed, when the m-FMSNs were further reacted with TMCS to graft the relatively small trimethylsilyl (TMS) groups, the *M*/*Q* ratio of the resulting sample (TMS-m-FMSN, *cf.* Figure 3) increased greatly to 12.0%. These results suggest that the bulky HDMS groups were mainly grafted onto the external surfaces of the m-FMSNs.

We performed phospholipid biofunctionalization using a modification of the method reported by Dubertret *et al.*[36] We suspect that the PEG-LipoFMSNs underwent self-assembly processes through hydrophobic interactions between HDMS groups and the fatty acyl chains of the phospholipid molecules. We also would like to emphasize here that HDMS groups were essential for a successful assembly of a phospholipid (or PEG-derived phospholipid) layer on the surface of m-FMSNs because the hydrocarbon chain of HDMS groups may

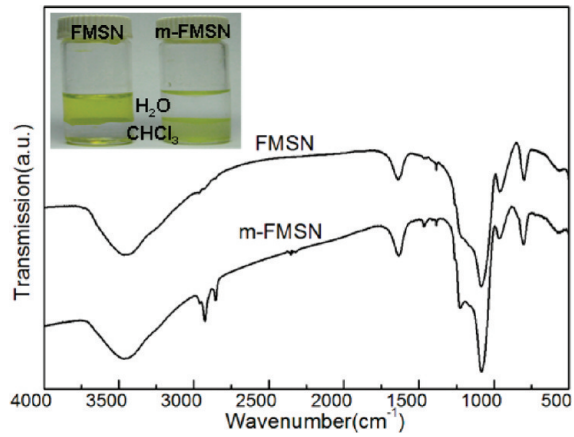

Figure 2. FTIR spectra of the FMSNs and m-FMSNs. Inset: Photograph of bare and modified FMSNs suspended in water and $CHCl_3$.

form a densely packed hydrophobic layer to stabilize the lipid layer. On the contrary, the surface anchored TMS groups, which were relatively small, failed to stabilize the phospholipids biofunctionalization, despite of their higher surface coverage than that of HDMS groups.

Unlike the m-FMSNs, the PEG-LipoFMSNs readily dispersed in aqueous solutions. We believe that phospholipid capping not only provided the FMSNs with a biofunctionalized surface but also prevented the FMSNs from aggregating in salt-containing solutions (Figure 4b). Dynamic light scattering (DLS) studies revealed the nature of the aggregation process on the microscopic scale (Figure 4a). Obviously, the average diameter of the PEG-LipoFMSNs remained stable for 24 h, whereas the control group (the bare FMSNs) aggregated in the salt-containing solution within a few hours. To further confirm the existence of the capping lipids on the outer surfaces of the FMSNs, we performed TEM with negative staining to examine the morphology and size of the mesoporous silica nanoshuttles before and after apply-

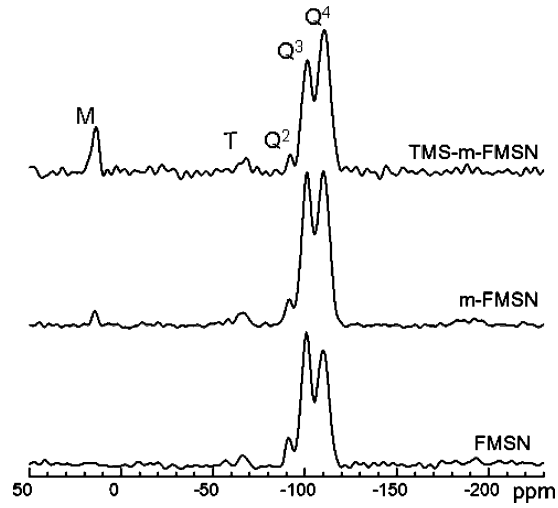

Figure 3. ^{29}Si MAS NMR spectra of the FMSNs, m-FMSNs, and TMS-m-FMSNs.

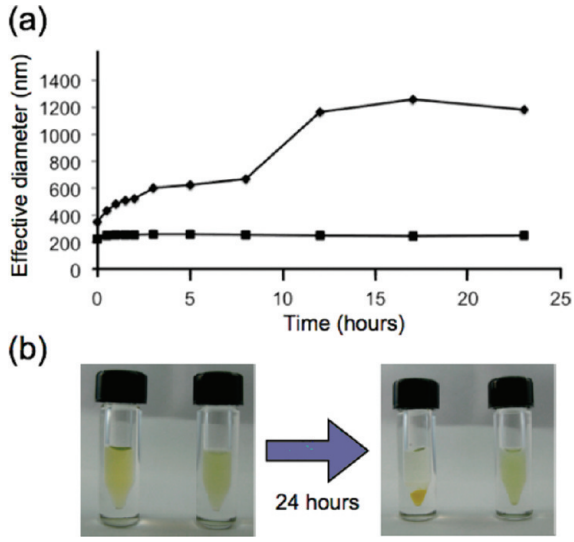

Figure 4. Aggregation phenomena of FMSNs in PBS observed using (a) DLS particle size analyzer (♦, bare; ■, lipid-capped) and (b) the naked eye.

ing the lipid coating. We used uranyl acetate as a staining agent; it is commonly used in TEM analyses of liposomes because of its ionic interactions with phospholipids. Figure 5a reveals an interpenetrating morphology for the FMSNs, presumably because of penetration of the uranyl acetate into the pores of the FMSNs. In contrast, the uranyl acetate molecules accumulated nonuniformly around the edges of the m-FMSNs (near the Cu grid) because the hydrophobic silane made the m-FMSNs much less hydrophilic, thereby reducing the degree of association between uranyl acetate and the m-FMSNs (Figure 5b) and blocking the uranyl acetate units from entering the pores of the FMSNs. Notably, the PEG-LipoFMSN revealed a totally different pattern after negative staining with uranyl acetate: a much more uniform coating over the FMSNs (Figure 5c), presumably because of the presence of the hydrophilic phosphate head groups of the lipids, which favored interactions with the uranyl acetate units.

In addition to their improved biofunctionality and suspensibility, our homemade PEG-LipoFMSNs exhibited repelling ability toward the protein immunoglobulin; this important feature of lipid capping has been used to protect fused-silica capillaries from nonspecific adsorption of proteins during capillary electrophoresis.[55] We performed this study by vortexing aliquots of IgG-FITC (0.1 mg mL^{-1}) with solutions (0.2 mg mL^{-1}) of the nonfluorescent MSNs and PEG-LipoMSNs, respectively. After incubation for 1 h, the MSNs were separated from the free fluorescent proteins (IgG-FITC) by centrifugation at 15000 rpm for 5 min, and then their supernatants were examined using fluorescence spectroscopy (Figure 6). As expected, the fluorescence intensity of the supernatant was higher for the system incorporating the PEG-LipoMSNs, indicating that the MSNs adsorbed more IgG-FITC nonspecifically (inset to Figure 6). From a comparison with the original fluorescence intensity of IgG-FITC (Ex, 496 nm; Em, 520 nm), the FL intensity in the supernatant obtained from the MSN group decreased by more than 70%, whereas that obtained from the PEG-LipoMSN group was reduced by only 25%. These results confirm that lipid capping protected the mesoporous silica nanoshuttles effectively from nonspecific protein adsorption.

Cellular Uptake and Cancer Cell Targeting. We investigated the uptake of various FMSNs [including bare FMSNs, PEG-LipoFMSNs, and folate-sensitized LipoFMSN (nanoshuttle@folate)] in Hela cells, a well-established cancer cell line with overexpressed folate receptors. For the purpose of cancer cell targeting, we modified the surfaces of our m-FMSNs with a combination of phospholipids (as described earlier) and a DSPE-PEG_{2000}-folic acid bioconjugate (0.4 mol %) to direct them to bind to the overexpressed folate receptors on the Hela cells. An immunoblotting study confirmed the successful incorporation of folate onto the FMSNs (see the Supporting Information).

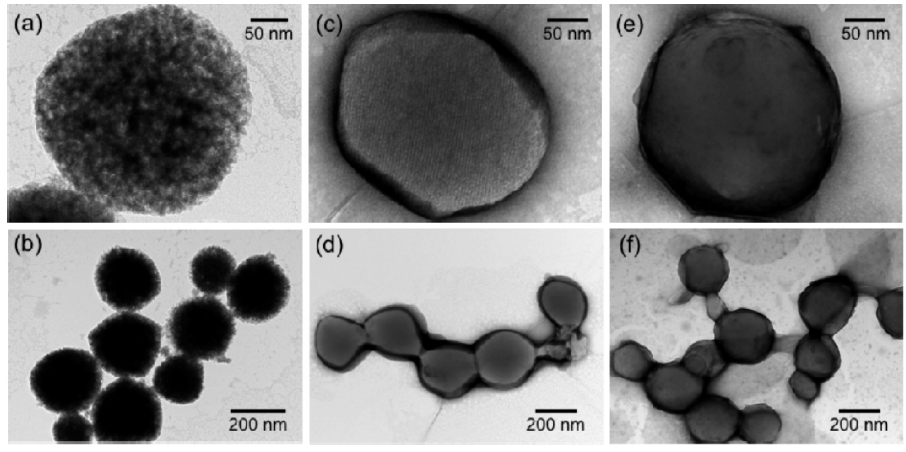

Figure 5. Uranyl acetate-stained TEM images of (a, b) the bare-FMSNs, (c, d) the m-FMSNs, and (e, f) the PEG-LipoFMSNs.

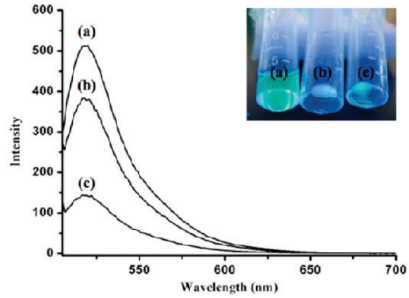

	% IgG being adsorbed non-specifically	Estimated total # of IgG being adsorbed non-specifically	Estimated # of adsorbed IgG per particle
Bare MSN	73.5%	1.47×10^{13}	1606
PEG-LipoMSN	26%	0.52×10^{13}	568

Figure 6. Fluorescence emission spectra for the supernatant of FITC-IgG solutions incubated with (a) no particles, (b) the lipid-capped MSNs, and (c) the bare-MSNs. Inset: Photograph of the fluorescent pellets after centrifugation. The quantitation of the amount of IgG bound to MSN particles was also provided.

After 24 h of cell attachment, the Hela cells were treated with the same concentrations of the FMSNs, the PEG-LipoMSNs, and the nanoshuttle@folate for 5 h (in serum-containing medium), followed by washing with PBS. The cell samples were then treated with trypan blue for 1 min to quench most of the green fluorescence contributed by the FMSNs sticking to the outer surfaces of the cell membranes; subsequently, we subjected them to analysis using fluorescence and confocal microscopies. As indicated in Figure 7a, uptake of the bareFMSNs occurred mostly through nonspecific binding (or adsorption); because the PEG-LipoMSNs were able to resist nonspecific adsorption, fewer particles were internalized (Figure 7d). On the other hand, the number of nanoparticles engulfed by the cells increased for the folate-directed nanoshuttles because of the specific binding between the folates and folate receptors on the Hela cells (Figure 7g). We obtained similar results from flow cytometry (Figure 7c,f,i). The confocal microscopy images (Figure 7j) revealed that the nanoshuttles crossed the cell membranes and became internalized within the cells. The green fluorescence of FITC was clearly evident in the cytoplasm. Because the green fluorescence of FITC appeared as localized, discrete dots, we suspect that these fluorescent molecules continued to reside within the MSNs, rather than leaching from them. In addition, the A549 cell line, which was often considered to have negative expression of folate receptor on its cell membrane, was selected as the control cell. The flow cytometric result of A549 cells incubated with nanoshuttles@folate (Figure 7k), confirming less nanoshuttles@folate were uptaken by the A549 (40% *vs* 99.06% of Hela cells as shown in Figure 7i). The cell densities were comparable for each of the incubated samples in Figure 7; therefore, the differences in fluorescence intensity arose from differences in the levels of association. The combination of ligand-mediated targeting with the tunable pore sizes and internal spaces present within phospholipid-functionalized mesoporous silica nanoparticles may offer a perfect solution for the development of drug and gene delivery vectors in biological systems.

SUMMARY

In this study, a platform procedure has been developed with the flexibility of anchoring multitypes of phospholipids to the surface of mesoporous silica nanoparticles (MSN) by hydrophobic CDSMH. In addition, we have also demonstrated a novel drug delivery system based on phospholipid-capped mesoporous silica nanoshuttles. Relative to their corresponding bare mesoporous silica materials, the biofunctionalized nanoparticles exhibited superior suspensibility in aqueous buffer solutions and greatly reduced nonspecific binding to cancer cells (Hela cells). Furthermore, a cell death assay revealed that the mesoporous silica nanoshuttles exerted no apparent cytotoxic effects on the Hela cells. Our results suggest that phospholipid capping holds great promise in (i) improving the aqueous suspensibility of mesoporous silica nanoshuttles under physiological conditions and (ii) protecting them against the nonspecific adsorption of proteins. It also implies that this new lipid-capped MSN nanoshuttles are talented novel drug vectors with potential clinical applicability. The bioadvantages of lipid-capped MSN nanoshuttles developed herein include the following: (i) the biocompatible phospholipid shell should provide better protection against opsonization[35,56] because of its anti-nonspecific protein binding effect; (ii) our lipid-capped MSN nanoshuttles prepared *via* the hydrophobic modification of CDSMH, are likely to result in larger density

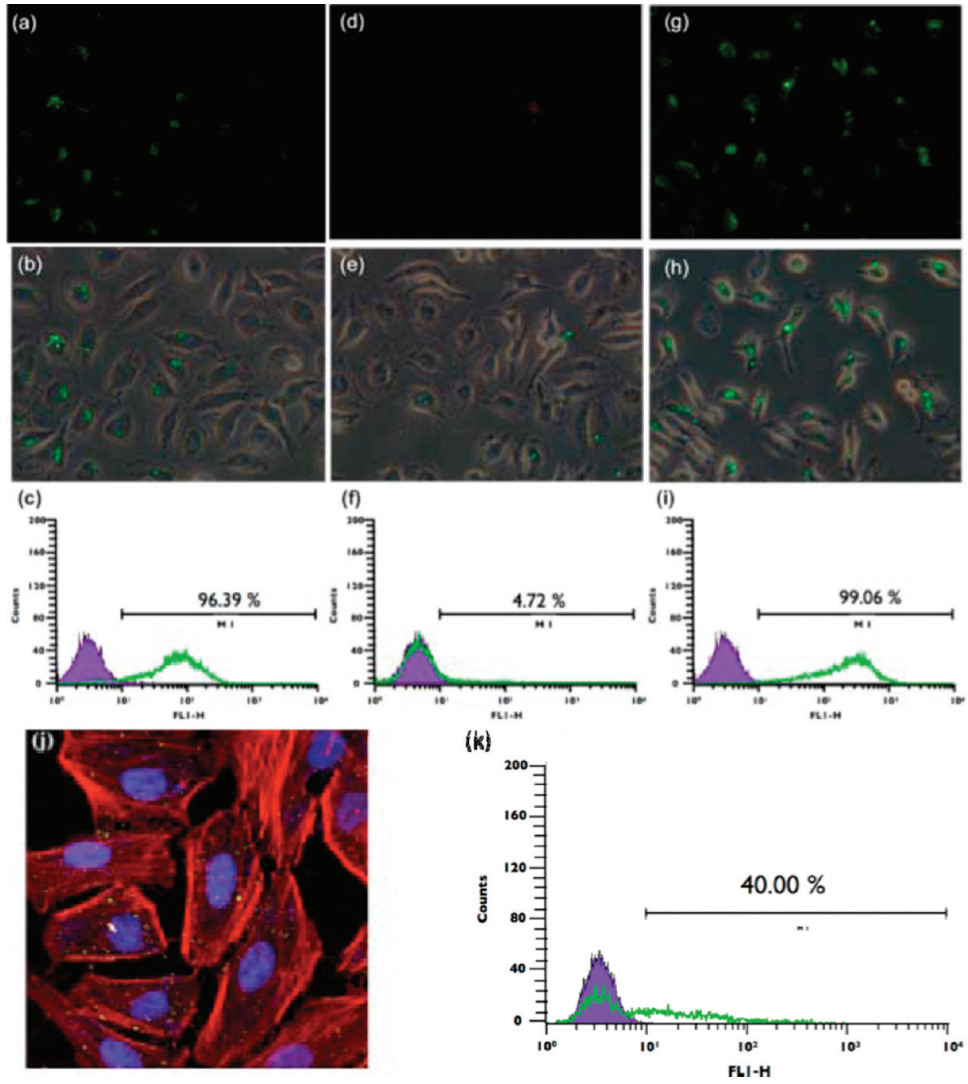

Figure 7. HeLa cancer cell uptake experiments of (a, b, c) the bare FMSNs, (d, e, f) the PEG-LipoMSNs, and (g, h, i) the nanoshuttles@folate. Each nanoshuttle (20 μg mL^{-1}) was incubated with the Hela cell for 5 h. (a, d, g) Fluorescence images; (b, e, h) merged images; (c, f, i) samples analyzed through flow cytometry, measuring the relative fluorescence intensity of FITC per cell at the FITC-A channel. (k) The flow cytometric result of A549 cells incubated with nanoshuttles@folate, confirming less nanoshuttles@folate were uptaken by the A549 (40% *vs* 99.06% of Hela cells as shown in panel i) due to the low-level folate receptor expression. (j) Confocal images of folate-sensitized LipoFMSNs (nanoshuttles@folate; green) in Hela cells; the cell skeleton was stained with rhodamine phalloidin (red); the nucleus was stained with DAPI (blue). Cells were incubated with the nanoshuttles@folate for 5 h.

coverage and better stability against aggregation, compared to low-density surface coating caused by the bulky molecule surface coating strategy. Ongoing studies are focusing on the demonstration of the loading of anticancer drugs into these therapeutic nanoshuttles, with the goal of minimizing toxic effects on healthy tissues while maintaining antitumor efficacy.

METHODS

Reagents, Materials, and Apparatus. All chemicals and organic solvents were of analytical grade or the highest purity commercially available; they were used as received. Aminopropyltriethoxysilane (APTES), cetyltrimethylammonium bromide (CTAB), $CHCl_3$, dicyclohexylcarbodiimide (DCC), dimethyl sulfoxide (DMSO), EtOH, fluorescein isothiocyanate (FITC), folic acid (FA), hydrogen chloride, hexane, IgG-FITC (affinity-purified antibody fluorescein-labeled goat antirabbit IgG), isopropyl ether, MeOH, potassium phosphate monobasic, KCl, pyridine, NaOH, NaCl, sodium phosphate dibasic, tetraethylorthosilicate (TEOS), and trypan blue were purchased from Sigma (St. Louis, MO). 13-(Chlorodimethylsilylmethyl)heptacosane (CDSMH) and trimethylchlorosilane (TMCS) were obtained from Gelest (Morrisville, PA). 1,2-Dihexadecanoyl-*sn*-glycero-3-phosphocholine (DPPC), 1,2-dipalmitoyl-*sn*-glycero-3-phosphoethanolamine-*N*-[methoxypoly (ethylene glycol)-2000] (DPPE-PEG_{2000}), and 1,2-distearoyl-*sn*-glycero-3-phosphoethanolamine-*N*-[aminopoly(ethylene glycol)-2000] (DSPE-PEG_{2000}-amine) were acquired from Avanti Polar Lipids (Alabaster, AL). Uranyl acetate was attained from Electron Microscopy Sciences (Hatfield, PA). Dulbecco's modified Eagle's medium (DMEM), penicillin/streptomycin solution, and trypsin were obtained

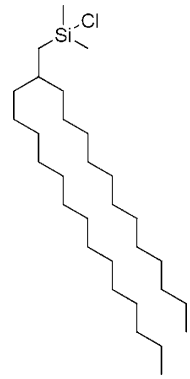

Scheme 1. Structure of 13-(chlorodimethylsilylmethyl)heptacosane (CDSMH).

from Hyclone (Logan, UT). Fetal bovine serum (FBS) was purchased from Biological Industries (Kibbutz Beit Haemek, Israel). All solutions were prepared with deionized water having a resistivity no less than 18 MΩ cm^{-1} (Milli-Q, Bedford, MA).

PXRD patterns were obtained on a Mac Science 18MPX diffractometer using Cu Kα radiation. Nitrogen physisorption isotherms were measured at 77 K using a Quantachrome Autosorb-1-MP instrument. FTIR spectra were acquired on a Perkin-Elmer Spectrum One B spectrometer; the washed and dried sample were dispersed into KBr and compressed into pellets. Solid state ^{29}Si magic-angle spinning (MAS) NMR spectra were acquired on a Bruker DSX400WB spectrometer using 4-mm MAS probes and a spinning rate of 6.5 kHz. ^{1}H NMR spectra were acquired on a Varian Unity Inova 600 (Cary, NC). TEM and SEM analyses were performed using a JEOL JEM-1400 instrument (Tokyo, Japan) operated at 120 kV and a JEOL JSM-7000F FESEM instrument (Tokyo, Japan) operated at 5 kV, respectively. The size distribution and zeta potential of the liposomes were measured using a 90Plus nanoparticle size analyzer and a ZetaPlus zeta potential analyzer, respectively (Brookhaven Instruments Corporation, Holtsville, NY).

Synthesis of FMSNs. The procedure for synthesizing the FMSNs was modified from the method reported by Mou *et al.*[10] A solution of FITC (8.6 mg) in EtOH (2 mL) was mixed with APTES (0.197 mL) and then the mixture was stirred at room temperature for 24 h to form the FITC-conjugated silane (FITC-Si). For the synthesis of the FMSNs, a surfactant solution was first prepared by dissolving CTAB (506 mg) in aqueous NaOH (9 mM, 400 mL). A solution of TEOS (0.448 mL) in EtOH (2.2 mL) was added into the surfactant solution, and the mixture was stirred for 1.5 h; FITC-Si was then added and the mixture stirred for a further 1 h. Finally, another solution of TEOS (1.792 mL) in EtOH (12 mL) was slowly added, and then the mixture was stirred for another 1 h before being aged at 60 °C for 24 h. The solid product was washed and filtered; the surfactant template molecules were removed under reflux in acidified EtOH for 12 h. The resulting FMSNs was collected and stored in EtOH prior to use.

DSPE-PEG_{2000}-FA Bioconjugate.[57,58] DSPE-PEG_{2000}-amine (33.6 mg), DCC (15.3 mg), and pyridine (167 μL) were added to a solution of FA (16.7 mg) in DMSO (667 mL) and then the mixture was left to react for 4 h at room temperature. After removing the pyridine under rotary evaporation, water (4.2 mL) was added to the solution. The product was dialyzed using a dialysis bag (MWCO: 12000−14000): twice against 50 mM NaCl (1 L) and three times against water (1 L). The solution was lyophilized to yield the final product (33.6 mg, 86%). ^{1}H NMR (δ): 0.87 (t, 6H, CH_3), 1.25 (s, 56H, CH_2), 1.53−1.65 (m, 4H, CH_2CH_2CO), 2.21−2.39 (m, 8H, CH_2CH_2CO and CH_2 of Glu), 3.40−3.49 (m, 4H, CH_2CH_2N), 3.64 (s, *ca.* 180H, PEG_{2000}), 4.35−4.37 (m, 1H, α-CH), 4.55 (d, 2H, 9-CH_2N), 5.20 (m, 1H, PO_4CH_2CH), 6.64 (d, 2H, 3′,5′-ArH), 7.68 (d, 2H, 2′,6′-ArH), 8.77 (s, 1H, C7−H).

Hydrophobization and Phospholipid Capping of FMSNs. The FMSNs (100 mg) were hydrophobized through treatment with a solution of CDSMH (1 mL, structure shown in Scheme 1) in $CHCl_3$ (50 mL) for 12 h. The resulting hydrophobic FMSNs (m-FMSNs) were washed with hexane and dried in air. For phospholipid capping of the m-FMSNs, a dispersion of the m-FMSNs in $CHCl_3$ (7 mg mL^{-1}, 1.0 mL) was added to a solution composed of DPPC and DPPE-PEG_{2000} (0.4 mol %) in a mixture of $CHCl_3$, isopropyl ether, and MeOH. After sonication for 3 min at 45 °C under a N_2 atmosphere, the organic solvent was evaporated from the mixture under reduced pressure. After adding PBS (7 mL), the mixture was sonicated at 90 W for 1 h. The biofunctionalized phospholipid-capped fluorescent mesoporous silica nanoshuttles (PEG-LipoFMSNs) were obtained after centrifugation at 15000 rpm for 5 min and washing with PBS (3 times) to remove excess uncapped lipids. The nanoshuttles were redispersed in PBS prior to use.

TEM and Dynamic Light Scattering (DLS). A drop of each sample (FMSN, m-FMSN, or PEG-LipoFMSN; 6 μL) was placed on a carbon-coated copper grid and dried at ambient temperature. For staining, a solution of 1% uranyl acetate (6 μL) was applied for 45 s and then it was removed through capillary action using filter paper; the grid was then dried and viewed under a JEOL JEM-1400 TEM operated at 120 kV. The size distribution and aggregation phenomena of the samples (such as, bare-FMSN and lipid-capped FMSN) suspended in salt-containing buffer were measured using dynamic light scattering (DLS) techniques (Brookhaven 90Plus nanoparticle size analyzer, equipped with a diode laser operated at 659 nm). A 20 μL portion of stock solution of particles (1 mg/mL) was added into 2 mL of PBS buffer, leading to the final concentration of around 9×10^8 particles of FMSN/mL.

***In Vitro* Targeting Experiments.** Hela cervical cancer cells (ATCC CCL-2) were cultured on six-well plates (Nunc, NY) in DMEM medium supplemented with 10% FBS and 1% PS in a standard incubator (5% CO_2; 37 °C). For all incubations, 1.0×10^5 cells of passage 15 were used for experiments ($n \geq 2$). The cells were incubated for 5 h with the PEG-LipoFMSNs or control FMSNs (bare) suspended in the medium at a concentration of 20 μg mL^{-1} and subjected to sonication for 30 min. Association between the various FMSNs and the Hela cells was evaluated using fluorescence and confocal microscopy, using an Olympus fluorescence microscope (IX-71, Olympus, Center Valley, PA) equipped with a 100-W halogen lamp and a confocal laser scanning microscope (LSM710-NLO, Zeiss, Munich, Germany). All fluorescence microscopy scans were performed using the same settings for the light source power and detector sensitivity, allowing direct comparison of the results obtained for the different incubations.

Acknowledgment. We thank the National Science Council of Taiwan for financial support under Grants NSC 98-2113-M-007-020-MY3 (Yang), 97-2113-M-260-006-MY2 (Wu), 98-2627-M-260-002 (Wu), 98-2113-M-007-013-MY3 (Ho), and 98-2627-M-006-012 (Ho).

Supporting Information Available: Immunoblotting study was conducted to confirm the presence of folate moieties on the surface of the nanoshuttles@folate. This material is available free of charge *via* the Internet at http://pubs.acs.org.

REFERENCES AND NOTES

1. Kresge, C. T.; Leonowicz, M. E.; Roth, W. J.; Vartuli, J. C.; Beck, J. S. Ordered Mesoporous Molecular Sieves Synthesized by a Liquid-Crystal Template Mechanism. *Nature* **1992**, *359*, 710–712.
2. Vallet-Regi, M.; Ramila, A.; del Real, R. P.; Perez-Pariente, J. A New Property of MCM-41: Drug Delivery System. *Chem. Mater.* **2001**, *13*, 308–311.
3. Mou, C. Y.; Lin, H. P. Control of Morphology in Synthesizing Mesoporous Silica. *Pure Appl. Chem.* **2000**, *72*, 137–146.
4. Huh, S.; Wiench, J. W.; Yoo, J. C.; Pruski, M.; Victor, S. Y. L. Organic Functionalization and Morphology Control of Mesoporous Silicas *via* a Co-Condensation Synthesis Method. *Chem. Mater.* **2003**, *15*, 4247–4256.
5. Sadasivan, S.; Khushalani, D.; Mann, S. Synthesis and Shape Modification of Organo-Functionalised Silica Nanoparticles

with Ordered Mesostructured Interiors. *J. Mater. Chem.* **2003**, *13*, 1023–1029.
6. Trewyn, B. G.; Whitman, C. M.; Lin, V. S. Y. Morphological Control of Room-Temperature Ionic Liquid Templated Mesoporous Silica Nanoparticles for Controlled Release of Antibacterial Agents. *Nano Lett.* **2004**, *4*, 2139–2143.
7. Gao, F.; Botella, P.; Corma, A.; Blesa, J.; Dong, L. Monodispersed Mesoporous Silica Nanoparticles with Very Large Pores for Enhanced Adsorption and Release of DNA. *J. Phys. Chem. B* **2009**, *113*, 1796–1804.
8. Hou, Z.; Theyssen, N.; Brinkmann, A.; Klementiev, K. V.; Grunert, W.; Buhl, M.; Schmidt, W.; Spliethoff, B.; Tesche, B.; Weidenthaler, C. Supported Palladium Nanoparticles on Hybrid Mesoporous Silica: Structure/Activity-Relationship in The Aerobic Alcohol Oxidation Using Supercritical Carbon Dioxide. *J. Catal.* **2008**, *258*, 315–323.
9. Martines, M. U.; Yeong, E.; Persin, M.; Larbot, A.; Voorhout, W. F.; Kubel, C. K. U.; Kooyman, P.; Prouzet, E.; Hexagonal Mesoporous Silica Nanoparticles with Large Pores and a Hierarchical Porosity Tested for HPLC, *C.R. Chim.* **2005**, *8*, 627–634.
10. Lin, Y.-S.; Tsai, C.-P.; Huang, H.-Y.; Kuo, C.-T.; Hung, Y.; Huang, D.-M.; Chen, Y.-C.; Mou, C.-Y. Well-Ordered Mesoporous Silica Nanoparticles as Cell Markers. *Chem. Mater.* **2005**, *17*, 4570–4573.
11. Rosenholm, J. M.; Meinander, A.; Peuhu, E.; Niemi, R.; Eriksson, J. E.; Sahlgren, C.; Linden, M. Targeting of Porous Hybrid Silica Nanoparticles to Cancer Cells. *ACS Nano* **2009**, *3*, 197–206.
12. Lu, J.; Liong, M.; Zink, J. I.; Tamanoi, F. Mesoporous Silica Nanoparticles as a Delivery System for Hydrophobic Anticancer Drugs. *Small* **2007**, *3*, 1341–1346.
13. Radu, D. R.; Lai, C. Y.; Wiench, J. W.; Pruski, M.; Lin, V. S. Y. Gatekeeping Layer Effect: A Poly(lactic acid)-Coated Mesoporous Silica Nanosphere-Based Fluorescence Probe for Detection of Amino-Containing Neurotransmitters. *J. Am. Chem. Soc.* **2004**, *126*, 1640–1641.
14. Lai, C. Y.; Trewyn, B. G.; Jeftinija, D. M.; Jeftinija, K.; Xu, S.; Jeftinija, S.; Lin, V. S. Y. A Mesoporous Silica Nanosphere-Based Carrier System with Chemically Removable CdS Nanoparticle Caps for Stimuli-Responsive Controlled Release of Neurotransmitters and Drug Molecules. *J. Am. Chem. Soc.* **2003**, *125*, 4451–4459.
15. Torney, F.; Trewyn, B. G.; Victor, S. Y. L.; Wang, K. Mesoporous Silica Nanoparticles Deliver DNA and Chemicals into Plants. *Nat. Nanotechnol.* **2007**, *2*, 295–300.
16. Giri, S.; Trewyn, B. G.; Stellmaker, M. P.; Lin, V. S. Y. Stimuli-Responsive Controlled-Release Delivery System Based on Mesoporous Silica Nanorods Capped with Magnetic Nanoparticles. *Angew. Chem., Int. Ed.* **2005**, *44*, 5038–5044.
17. Radu, D. R.; Lai, C. Y.; Jeftinija, K.; Rowe, E. W.; Jeftinija, S.; Victor, S. Y. L. Gatekeeping Layer Effect: A Poly(lactic acid)-Coated Mesoporous Silica Nanosphere-Based Fluorescence Probe for Detection of Amino-Containing Neurotransmitters. *J. Am. Chem. Soc.* **2004**, *126*, 13216–13217.
18. Taylor, K. M. L.; Kim, J. S.; Rieter, W. J.; An, H.; Lin, W.; Lin, W. Mesoporous Silica Nanospheres as Highly Efficient MRI Contrast Agents. *J. Am. Chem. Soc.* **2008**, *130*, 2154–2155.
19. Tsai, C. P.; Hung, Y.; Chou, Y. H.; Huang, D. M.; Hsiao, J. K.; Chang, C.; Chen, Y. C.; Mou, C. Y. High-Contrast Paramagnetic Fluorescent Mesoporous Silica Nanorods as a Multifunctional Cell-Imaging Probe. *Small* **2008**, *4*, 186–191.
20. Wu, S. H.; Lin, Y. S.; Hung, Y.; Chou, Y. H.; Hsu, Y. H.; Chang, C.; Mou, C. Y. Multifunctional Mesoporous Silica Nanoparticles for Intracellular Labeling and Animal Magnetic Resonance Imaging Studies. *ChemBioChem* **2008**, *9*, 53–57.
21. Liong, M.; Lu, J.; Kovochich, M.; Xia, T.; Ruehm, S. G.; Nel, A. E.; Tamanoi, F.; Zink, J. I. Multifunctional Inorganic Nanoparticles for Imaging, Targeting, and Drug Delivery. *ACS Nano* **2008**, *2*, 889–896.
22. Slowing, I. I.; Vivero-Escoto, J. L.; Wu, C. W.; Lin, V. S. Y. Mesoporous Silica Nanoparticles as Controlled Release Drug Delivery and Gene Transfection Carriers. *Adv. Drug Deliver. Rev.* **2008**, *60*, 1278–1288.
23. Slowing, I. I.; Trewyn, B. G.; Lin, V. S. Y. Mesoporous Silica Nanoparticles for Intracellular Delivery of Membrane-Impermeable Proteins. *J. Am. Chem. Soc.* **2007**, *129*, 8845–8849.
24. van Schooneveld, M. M.; Vucic, E.; Koole, R.; Zhou, Y.; Stocks, J.; Cormode, D. P.; Tang, C. Y.; Gordon, R. E.; Nicolay, K.; Meijerink, A.; *et al*. Improved Biocompatibility and Pharmacokinetics of Silica Nanoparticles by Means of a Lipid Coating: A Multimodality Investigation. *Nano Lett.* **2008**, *8*, 2517–2525.
25. Lai, C. W.; Wang, Y. H.; Lai, C. H.; Yang, M. J.; Chen, C. Y.; Chou, P. T.; Chan, C. S.; Chi, Y.; Chen, Y. C.; Hsiao, J. K. Iridium-Complex-Functionalized Fe_3O_4/SiO_2 Core/Shell Nanoparticles: A Facile Three-in-One System in Magnetic Resonance Imaging, Luminescence Imaging, and Photodynamic Therapy. *Small* **2008**, *4*, 218–224.
26. Barbè, C.; Bartlett, J.; Kong, L.; Finnie, K.; Lin, H. Q.; Larkin, M.; Calleja, S.; Bush, A.; Calleja, G. Silica Particles: A Novel Drug-Delivery System. *Adv. Mater.* **2004**, *16*, 1959–1966.
27. Borchardt, G.; Brandriss, S.; Kreuter, J.; Margel, S. Body Distribution of 75Se-Radiolabeled Silica Nanoparticles Covalently Coated with Co-Functionalized Surfactants after Intravenous Injection in Rats. *J. Drug Target.* **1994**, *2*, 61–77.
28. Kim, J.; Lee, J. E.; Lee, J.; Youngjin, J.; Sang-Wook, K.; Kwangjin, A.; Ho, Y. J.; Taeghwan, H. Generalized Fabrication of Multifunctional Nanoparticle Assemblies on Silica Spheres. *Angew. Chem., Int. Ed.* **2006**, *45*, 4789–4793.
29. Kumar, R.; Roy, I.; Ohulchanskyy, T. Y.; Goswami, L. N.; Bonoiu, A. C.; Bergey, E. J.; Tramposch, K. M.; Maitra, A.; Prasad, P. N. Covalently Dye-Linked, Surface-Controlled, and Bioconjugated Organically Modified Silica Nanoparticles as Targeted Probes for Optical Imaging. *ACS Nano* **2008**, *2*, 449–456.
30. Bagwe, R. P.; Hilliard, L. R.; Tan, W. Surface Modification of Silica Nanoparticles to Reduce Aggregation and Nonspecific Binding. *Langmuir* **2006**, *22*, 4357–4362.
31. Huo, Q.; Liu, J.; Wang, L. Q.; Jiang, Y.; Lambert, T. N.; Fang, E. A New Class of Silica Cross-Linked Micellar Core−Shell Nanoparticles. *J. Am. Chem. Soc.* **2006**, *128*, 6447–6453.
32. Jo, S.; Park, K. Surface Modification Using Silanated Poly(Ethylene Glycol)s. *Biomaterials.* **2000**, *21*, 605–616.
33. Yang, C. Y.; Cai, S. J.; Liu, H.; Pidgeon, C. Immobilized Artificial Membranes−Screens for Drug Membrane Interactions. *Adv. Drug Delivery Rev.* **1997**, *23*, 229–256.
34. Liu, J.; Stace-Naughton, A.; Jiang, X.; Brinker, C. J. Porous Nanoparticle Supported Lipid Bilayers (Protocells) as Delivery Vehicles. *J. Am. Chem. Soc.* **2009**, *131*, 1354–1355.
35. Moghimi, S. M.; Hunter, A. C.; Murray, J. C. Long-Circulating and Target-Specific Nanoparticles: Theory to Practice. *Pharmacol. Rev.* **2001**, *53*, 283–318.
36. Dubertret, B.; Skourides, P.; Norris, D. J.; Noireaux, V.; Brivanlou, A. H.; Libchaber, A. *In Vivo* Imaging of Quantum Dots Encapsulated in Phospholipid Micelles. *Science* **2002**, *298*, 1759–1762.
37. Fan, H.; Leve, E. W.; Scullin, C.; Gabaldon, J.; Tallant, D.; Bunge, S.; Boyle, T.; Wilson, M. C.; Brinker, C. J. Surfactant-Assisted Synthesis of Water-Soluble and Biocompatible Semiconductor Quantum Dot Micelles. *Nano Lett.* **2005**, *5*, 645–648.
38. Sitaula, S.; Mackiewicz, M. R.; Reed, S. M. Gold Nanoparticles Become Stable to Cyanide Etch When Coated with Hybrid Lipid Bilayers. *Chem. Commun.* **2008**, 3013–3015.
39. Lim, Y. T.; Lee, K. Y.; Lee, K.; Chung, B. H. Immobilization of Histidine-Tagged Proteins by Magnetic Nanoparticles Encapsulated with Nitrilotriacetic Acid (NTA)-Phospholipids Micelle. *Biochem. Biophys. Res. Commun.* **2006**, *344*, 926–930.
40. Park, J. H.; Maltzahn, G. V.; Ruoslahti, E.; Bhatia, S. N.; Sailor,

M. J. Micellar Hybrid Nanoparticles for Simultaneous Magnetofluorescent Imaging and Drug Delivery. *Angew. Chem., Int. Ed.* **2008**, *47*, 7284–7288.
41. Zhang, L.; Chan, J. M.; Gu, F. X.; Rhee, J. W.; Wang, A. Z.; Radovic-Moreno, A. F.; Alexis, F.; Langer, R.; Farokhzad, O. C. Self-Assembled Lipid-Polymer Hybrid Nanoparticles: A Robust Drug Delivery Platform. *ACS Nano* **2008**, *2*, 1696–1702.
42. Leamon, C. P.; Low, P. S. Folate-Mediated Targeting: From Diagnostics to Drug and Gene Delivery. *Drug Discovery Today* **2001**, *6*, 44–51.
43. Leamon, C. P.; Reddy, J. A. Folate-Targeted Chemotherapy. *Adv. Drug Delivery Rev.* **2004**, *56*, 1127–1141.
44. Elnakat, H.; Ratnam, M. Distribution, Functionality and Gene Regulation of Folate Receptor Isoforms: Implications in Targeted Therapy. *Adv. Drug Delivery Rev.* **2004**, *56*, 1067–1084.
45. Sudimack, J.; Lee, R. J. Targeted Drug Delivery *via* the Folate Receptor. *Adv. Drug Delivery Rev.* **2000**, *41*, 147–162.
46. Magee, W. E.; Miller, O. V. Liposomes Containing Antiviral Antibody Can Protect Cells from Virus Infection. *Nature* **1972**, *235*, 339–341.
47. Mayhew, E.; Ito, M.; Lazo, R. Toxicity of Non-drug-Containing Liposomes for Cultured Human Cells. *Exp. Cell Res.* **1987**, *171*, 195–202.
48. Adams, D. H.; Joyce, G.; Richardson, V. J.; Ryman, B. E.; Wisniewski, H. M. Liposome Toxicity in the Mouse Central Nervous System. *J. Neurol. Sci.* **1977**, *31*, 173–179.
49. Jeong, M. W.; Oh, S. G.; Kim, Y. C. Effects of Amine and Amine Oxide Compounds on the Zeta-Potential of Emulsion Droplets Stabilized by Phosphatidylcholine. *Colloids Surf. A* **2001**, *181*, 247–253.
50. Lowell, S. *Characterization of Porous Solids and Powders: Surface Area, Pore Size, and Density*; Kluwer Academic Press, New York, 2004.
51. Yang, C. M.; Sheu, H. S.; Chao, K. J. Templated Synthesis and Structural Study of Densely Packed Metal Nanostructures in MCM-41 and MCM-48. *Adv. Funct. Mater.* **2002**, *12*, 143–148.
52. Yang, C. M.; Liu, P. H.; Ho, Y. F.; Chiu, C. Y.; Chao, K. J. Highly Dispersed Metal Nanoparticles in Functionalized SBA-15. *Chem. Mater.* **2003**, *15*, 275–280.
53. Yang, C. M.; Lin, H. A.; Zibrowius, B.; Spliethoff, B.; Schuth, F.; Liou, S. C.; Chu, M. W.; Chen, C. H. Selective Surface Functionalization and Metal Deposition in the Micropores of Mesoporous Silica SBA-15. *Chem. Mater.* **2007**, *19*, 3205–3211.
54. Lin, H. A.; Liu, C. H.; Huang, W. C.; Liou, S. C.; Chu, M. W.; Chen, C. H.; Lee, J. F.; Yang, C. M. Novel Magnetically Separable Mesoporous Fe_2O_3@SBA-15 Nanocomposite with Fully Open Mesochannels for Protein Immobilization. *Chem. Mater.* **2008**, *20*, 6617–6622.
55. Mansfield, E.; Ross, E. E.; D'Ambruoso, G. D.; Keogh, J. P.; Huang, Y.; Aspinwall, C. A. Fabrication and Characterization of Spatially Defined, Multiple Component, Chemically Functionalized Domains in Enclosed Silica Channels Using Cross-Linked Phospholipid Membranes. *Langmuir* **2007**, *23*, 11326–11333.
56. Gref, R.; Domb, A.; Quellec, P.; Blunk, T.; Muller, R. H.; Verbavatz, J. M.; Langer, R. The Controlled Intravenous Delivery of Drugs Using PEG-Coated Sterically Stabilized Nanospheres. *Adv. Drug Delivery Rev.* **1995**, *16*, 215–233.
57. Gabizon, A.; Horowitz, A. T.; Goren, D.; Tzemach, D.; Mandelbaum-Shavit, F.; Qazen, M. M.; Zalipsky, S. Targeting Folate Receptor with Folate Linked to Extremities of Poly(ethylene glycol)-Grafted Liposomes: *In Vitro* Studies. *Bioconjugate Chem.* **1999**, *10*, 289–298.
58. Ho, J. A. A.; Hung, C. H.; Wu, L. C.; Liao, M. Y. Folic Acid-Anchored PEGgylated Phospholipid Bioconjugate and Its Application in a Liposomal Immunodiagnostic Assay for Folic Acid. *Anal. Chem.* **2009**, *81*, 5671–5677.